JET PROPULSION LABORATORY INTEROFFICE MEMORANDUM

3411-95-235csi

June 26, 1995

TO: J. Yu

FROM: J. W. Melody

SUBJECT: SONATA Integrated Model and Open-Loop Disturbance Analysis

SUMMARY:

This memo summarizes the integrated structural-optical model of SONATA created in IMOS. The model is used to find the open-loop stellar interferometer optical pathlength difference and total differential wavefront tilt variations resulting from reaction wheel force and torque disturbances, as a function of wheel speed. The open-loop disturbance analysis investigates the effectiveness of vibration isolation and structural quieting at disturbance attenuation.

Distribution:

G. Blackwood
R. Calvet
M. Colavita
R. Laskin
K. Lau
M. Levine-West
J. McGuire
M. Milman
G. Neat
L. Needels
J. O'Brien
G. Sevaston
S. Shaklan
M. Shao
J. Spanos
R. Stanton
F. Tolivar
S. Wilson
D. Wolff

Introduction

A fundamental technical challenge for large-baseline distributed-optics spacecraft is to maintain the relative position of optical elements mounted on a lightweight and relatively soft structure. The proposed solution has been to use a layered control methodology consisting of: 1) disturbance isolation, 2) structural quieting, and 3) high bandwidth optical control [1]. The first layer either seeks to attenuate the disturbances entering the structure (the "noisy box" application) or it isolates a payload from the structure ("quiet box" application) [2]. The second layer quiets the structure by replacing truss members with damping struts, performing two functions: reducing the disturbance transmitted through the structure and conditioning the plant for the optical control systems. The third layer actively rejects the residual disturbances observable in the optical output. The effectiveness of the isolation layer and the disturbance attenuation function of the structural quieting layer is assessed for SONATA in the following analysis.

An integrated structural-optical model of SONATA has been created in order to predict open-loop and closed-loop performance and thereby to evaluate the proposed layered control architecture. This modeling was performed in Matlab, using the Integrated Modeling of Optical Systems (IMOS) toolbox developed at JPL.

This memo describes the open-loop disturbance analysis used to evaluate the effectiveness of the isolation layer and the disturbance attenuation function of the structural quieting layer. This analysis is performed for three cases: 1) no isolation with no structural quieting, 2) isolation with no structural quieting, and 3) no isolation with structural quieting.

The analysis incorporates a Hubble Space Telescope (HST) reaction wheel disturbance model [3]. Given this disturbance model, the steady state stellar optical pathlength difference (OPD) and stellar differential wavefront tilt (DWT) variations are calculated for a range of reaction wheel speeds. An intrinsic modal damping of 0.1% is assumed. Structural quieting is modeled by increasing the modal damping to 5%. When isolated, the reaction wheel is assumed to be isolated in all six degrees of freedom, consistent with a hexapod isolator. The model uses a passive isolator with a cutoff frequency of 4 Hz.

Structural Finite Element Geometry

The finite element geometry of SONATA is shown in Figure 1. The model includes the instrument truss, the spacecraft bay truss, the solar panel, and the optical plates. For the sake of clarity, the instrument and spacecraft bay trusses are shown separately in Figure 2.

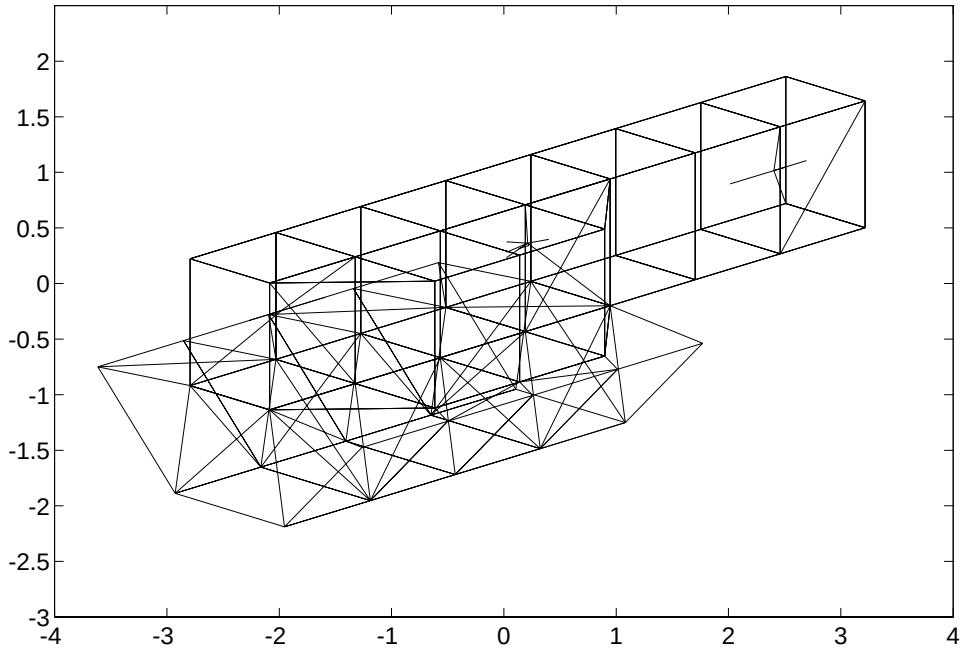

Figure 1: SONATA Finite Element Geometry

Truss Geometry

The instrument truss is the rectangular truss that runs the length of the model. This truss holds the three optical plates, and is composed of aluminum beams and plate elements [4]. The plate elements are placed around the outside of the truss and between the bays of the truss. The beams are assumed to be radially symmetric with a crossectional area of $1.9\text{x}10^{-4}$ m^2 and a bending moment of inertia $5.78\text{x}10^{-8}$ m^4. The plates are modeled as honeycomb sandwich with sheet thickness of 16 mils and a plate thickness of 1/4 inch.

The spacecraft bus is the trapezoidal truss structure at one end of the instrument truss. This bus houses the spacecraft flight system hardware. Of particular concern are the reaction wheel assemblies (RWAs) since they emit the only significant mechanical disturbances. The spacecraft bus is a truss covered with sandwich plate using the same properties as the instrument truss.

Solar Panel Geometry

The solar panel is attached to and acts as a shield for the spacecraft bus. The solar panel is three sides of an octagonal cylinder and is attached to the bus at its edges with beam elements. The solar panel itself is made up of plate elements. For simplicity, the solar

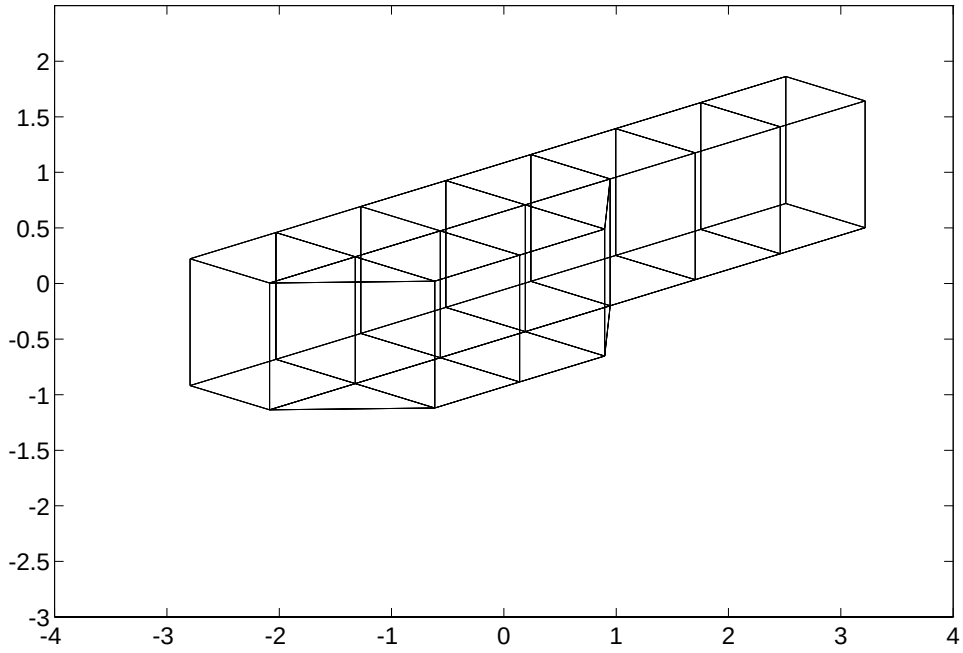

Figure 2: SONATA Spacecraft Bus and Instrument Truss Finite Element Geometry

panel plates and support truss beams are assumed to have properties similar to those of the instrument truss.

Optics Plate Geometries

The three optics plates are located two at either end of the instrument truss and one in the center. The end plates contain the siderostats and the beam compressors, whereas the center plate holds the delay lines, the beam combiner, and the detector. The plates are modeled with rigid body elements (RBEs). The center of mass of each plate is connected to several truss nodes of the nearest bay using RBE3 elements. The RBE3 element finds the average motion (in a least squares sense) of the several truss nodes and assigns this motion to the plate center of mass. The optics nodes are then connected by an RBE2 to the plate center of mass. The RBE2 constrains motion of one node by the motion of another node, modeling a perfectly rigid connection. The plates are assumed to be rigid in order to limit the size of the model.

SONATA will have two wavefront tilt actuators for each interferometer arm, one two-axis siderostat and one two-axis fast steering mirror. For simplicity, only one two-axis actuator is modeled for each interferometer arm. The actuators are located on the end

plates and have a mass of 0.5 kg and inertias of 6.25x10^{-4} kgm^2 (spin axis) and 3.13x10^{-4} kgm^2 (tip/tilt axes). The mirrors are assumed to be mounted flexibly in all six degrees of freedom, with a resonance of 500 Hz. This frequency was chosen to model a fast steering mirror actuated by a set of PZT stacks, since this is the critical actuator in the wavefront tilt control system.

SONATA will have four optical delay lines, one for each interferometer associated with a quadrant of the narrow field. Since only three interferometers are essential for modeling the OPD feed forward (*i.e.*, two guide interferometers and one science interferometer), only three delay lines are modeled. The delay line models are based on the MPI delay lines. Each delay line is mounted on a flexure with a resonance of 1.15 Hz. Furthermore, they each have an internal defocus mode at 500 Hz and a PZT stack resonance mode at 4 kHz. The total delay line mass is 7.7 kg, with 5.5 kg mounted on the flexure. Two levels of actuation are modeled: the voice coil moving the flexibly mounted primary and secondary mirror support structure (a.k.a., "cat's eye"), and the reactionless PZT actuating the secondary mirror.

The open-loop disturbance analysis described in this memo assumes that the fast steering mirrors and the delay lines are rigid, in order to discern the magnitude of the disturbance problem for SONATA without control. The flexibilities are not included since they are inherent to the closed loop actuators. The flexibilities will be included in the closed-loop analysis.

Modal Solution

Once the finite element geometry and properties are specified, the element mass and stiffness matrices are assembled into the system mass and stiffness matrices. This includes concentrated masses (CONMs) of the optics and of the spacecraft flight system hardware. The result is a second order state space description of the form:

$$M\ddot{d} + Kd = B_f f \tag{1}$$

where M and K are the system mass and stiffness matrices, d is the nodal state, f is a vector of force input, and B_f is the force influence matrix.

After the system mass and stiffness matrices are built, multi-point constraints are generated using the RBE elements. These constraints take the form of:

$$d = \begin{bmatrix} d_n \\ d_m \end{bmatrix} = \begin{bmatrix} I_n \\ G_m \end{bmatrix} d_n = G d_n \tag{2}$$

where d_n are the independent degrees of freedom and d_m are the dependent degrees of freedom. These constraints are then applied to Eq. 1, reducing the state of the system to

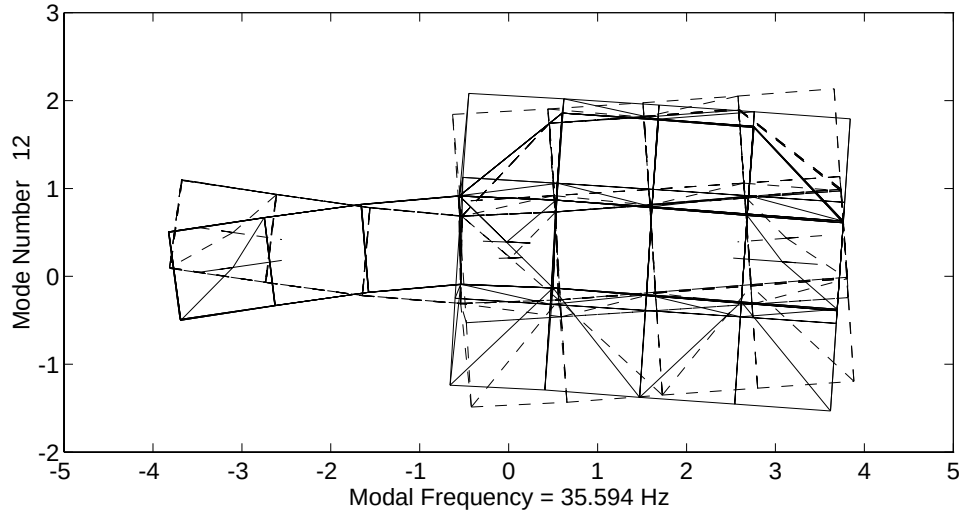

Figure 3: SONATA Lowest Global Flexible-Body Modeshape

the independent degrees of freedom:

$$\begin{aligned} G^T M G \ddot{d}_n + G^T K G d_n &= G^T B_f f \\ M_{nn} \ddot{d} + K_{nn} d &= B_{nf} f \end{aligned} \tag{3}$$

The eigensolution of Eq. 3 is found, yielding rigid-body and flexible body modes and modeshapes. The lowest global flexible body modeshape is shown in Figure 3. The resultant diagonalized system is:

$$\begin{aligned} \ddot{\eta} + 2Z\Omega\dot{\eta} + \Omega^2\eta &= \Phi_n^T B_{nf} f \\ d &= G\Phi_n \eta \end{aligned} \tag{4}$$

where η is the modal state vector, Z is a diagonal modal damping matrix, Ω is the diagonal modal frequency matrix, and Φ_n is the eigenvector matrix. Z is formed by assuming a uniform modal damping of 0.1% for all flexible body modes except the delay line flexure modes. When the delay line flexure modes are included in the model, they have 5% modal damping.

Stellar and Internal Metrology Optical Prescriptions

Two optical prescriptions were generated for the SONATA model: a prescription of the stellar interferometer for modeling stellar OPD, wavefront tilt, and DWT and 2) a prescription of the internal metrology system for modeling internal OPD measurement. Each

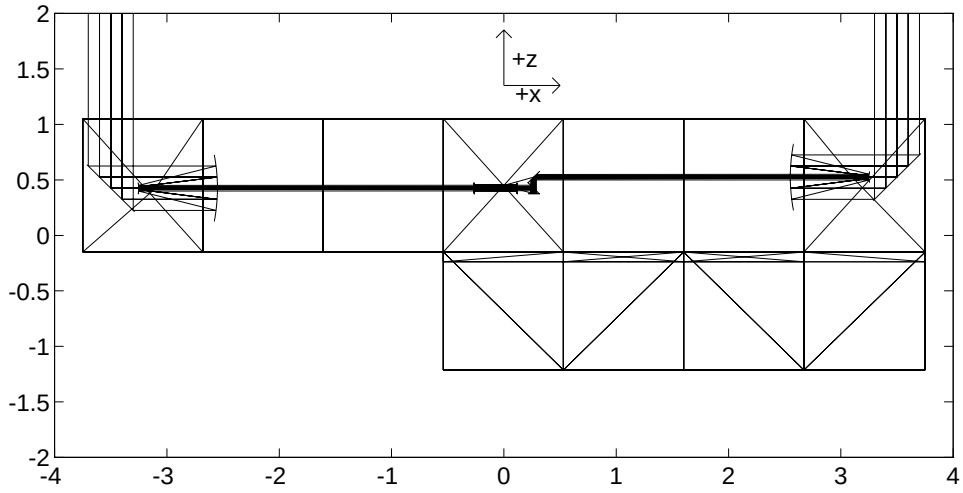

Figure 4: SONATA Stellar Interferometer Optical Prescription

of the two prescriptions is used three times for the three different interferometers mentioned above. Each prescription was specified and plotted in IMOS.

A ray trace of the stellar interferometer prescription is shown in Figure 4. The first mirror in the optical train is the siderostat mirror. This mirror is used as the actuator for the wavefront tilt control system as mentioned above. The starlight aperture is 0.4 m. Just after the siderostat is the starlight beam compressor with a compression ratio of 8 and an f/# of 2. Next in the beam train of the left interferometer is the delay line, modeled as flat mirrors for simplicity. The light strikes the flat "primary" (closest to the beam combiner), then the flat "secondary," back to the primary, and finally strikes a fixed "fold" mirror that directs it to the beam combiner. The fold mirror is coincident with the secondary mirror, but is attached to the optics plate directly. In this way, the effect on OPD of voice coil and PZT actuation are accurately modeled, *i.e.*, voice coil and PZT actuation cause an OPD of twice the motion. The inaccuracy of the model due to the flat delay line mirrors is in the absence of second-order defocus effects attendant to secondary mirror actuation and second-order effects of cat's eye rotation.

The internal metrology prescription is shown in Figure 5. This prescription has its input plane, the plane where the light originates, connected to the structure at the stellar interferometer detector location [5]. Beginning here, the light is traced down the optical train in the direction opposite that of the stellar interferometer. The optical elements are the same, albeit in reverse order, until after the beam compressor. At this point the internal metrology strikes a cornercube retro-reflector instead of the siderostat mirror and is reflected back down the optical train to a detector coincident with the input plane.

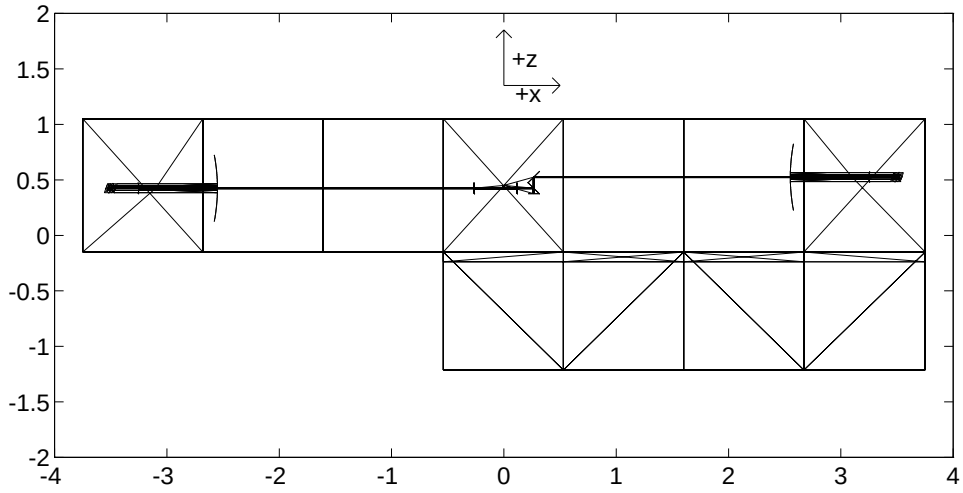

Figure 5: SONATA Internal Metrology Optical Prescription

Linear Optical Model

Once the optical prescriptions are generated, they are exported to COMP, where linear optical models are created [5]. These linear models are calculated by performing an analytic *differential* ray trace. The result is a model of the form:

$$y = C_{opt} d \tag{5}$$

where d is a vector of optical element position and orientation perturbations, y is a vector of optical output, and C_{opt} is the optical sensitivity matrix, commonly known as the "C-matrix" to COMP aficionados. The optical output can be differential pathlength, wavefront tilt, or spot motion.

A linear model was created for each optical prescription. The output of the stellar interferometer model is stellar OPD variation, stellar wavefront tilt variation for each arm of the interferometer about two axes, and the DWT between the two arms of the interferometer (about two axes). The output of the internal metrology model is internal OPD.

Integrated Structures-Optics Model

Once the structural modal model and the linear optical models have been created, they are integrated to form a structures-optics model. The structural model is first truncated according to the influence of the modes in the disturbance-to-optical output transfer functions using Hankel singular values. This resultant model includes correction vectors that

account for the stiffness of the modes lost in the truncation. Next the model is converted into first-order state space form enabling the use of standard Matlab analysis functions. Finally, the input and output are manipulated to include not only the disturbances and stellar optical metrics, but also the sensor output and actuator input for the pathlength, wavefront tilt, and attitude control systems. The resulting model is available for open-loop and closed-loop disturbance analyses.

Model Reduction

In order to reduce the size of the model, the modes are truncated according to their influence in the end-to-end transfer functions. This influence is measured by the Hankel singular value (known as "second-order mode" of the internally balanced realization in [6]) associated with each modeshape. In this case, the Hankel singular values, γ_i, are:

$$\begin{aligned} \gamma_i &= \frac{\sqrt{(b_{mi} b_{mi}^T)\,(c_{mi}^T c_{mi})}}{4\zeta^i \omega_i^2} \\ B_m &= \Phi_n^T G^T B_f \\ C_m &= C_{opt} G \Phi_n \end{aligned} \tag{6}$$

where ζ^i and ω_i are the damping and frequency associated with mode i, b_{mi} is the i^{th} row of B_m, and c_{mi} is the i^{th} column of C_m.

The model was truncated to include the six rigid body modes, all fast steering mirror and delay line dynamics, and the 30 most influential of the remaining flexible body modes. B_f was chosen so that the input, f, are forces and torques at the reaction wheel node.

In order to account for the low frequency stiffness of the eliminated modes, static correction vectors are included in the set of kept modeshapes. A static correction vector (a.k.a. a Ritz vector in [7]) is found for each input of f. In [8] the correction vectors are calculated according to:

$$\Phi_c = K^{-1} B - \Phi_k^T \Omega_k^{-2} \Phi_k B \tag{7}$$

where K is the system stiffness matrix, B is the force influence matrix, Ω_k and Φ_k are the modes and modeshapes of the kept modes, and Φ_c are the correction vectors.

In the case of the SONATA model however, K_{nn} is not invertible since the model has rigid body modes. Instead of calculating the overall static solution and subtracting the component associated with the kept modeshapes, the component of the static solution related to the lost modeshapes is found directly:

$$\Phi_c = \Phi_t^T \Omega_k^{-2} \Phi_t B \tag{8}$$

where Φ_t are the modeshapes lost in the truncation (*i.e.*, truncated modeshapes).

Incorporating the multi-point constraints, the correction vectors for SONATA are calculated according to:

$$\Phi_{nc} = \Phi_{nt}^T \Omega_k^{-2} \Phi_{nt} G^T B_f \tag{9}$$

where Φ_{nt} is a matrix of truncated modeshapes (independent dofs only), Ω_k is the corresponding modal frequency matrix, and Φ_{nc} is a matrix of the correction vectors.

First-Order State Space Model

The truncated modal model is then converted into first-order form by using the substitution:

$$x = \begin{bmatrix} \eta_r \\ \dot{\eta}_r \end{bmatrix} \tag{10}$$

Resulting in:

$$\begin{aligned} \dot{x} &= Ax + Bu \\ \begin{bmatrix} d \\ \dot{d} \end{bmatrix} &= C_d x + Du \end{aligned} \tag{11}$$

with:

$$\begin{aligned} A &= \begin{bmatrix} 0 & I \\ -2Z_r\Omega_r & -\Omega_r^2 \end{bmatrix} \quad B = \begin{bmatrix} 0 \\ \Phi_{nr}^T G^T B_f \end{bmatrix} \\ C_d &= \begin{bmatrix} G\Phi_{nr} & 0 \\ 0 & G\Phi_{nr} \end{bmatrix} \qquad D = 0 \end{aligned} \tag{12}$$

where the subscript r refers to the set of kept modeshapes and correction vectors:

$$\begin{aligned} \Omega_r &= \begin{bmatrix} 0 & 0 \\ 0 & \Omega_k \end{bmatrix} \quad Z_r = \begin{bmatrix} 0 & 0 \\ 0 & Z_k \end{bmatrix} \\ \Phi_{nr} &= \begin{bmatrix} \Phi_{nc} & \Phi_{nk} \end{bmatrix} \end{aligned} \tag{13}$$

and Z_k is the modal damping associated with the kept modal state.

Input and Output Manipulation

Reaction wheel disturbance input and stellar OPD and DWT output are required for the disturbance analysis. In order to enable closed-loop modeling, actuator input and sensor output must be included. Actuator input are tip-tilt torques of the fast steering mirrors, reactionless PZT forces and voice coil forces of the delay lines, and attitude control torques. Sensor output are angular position and rate at the node where the inertial reference unit is located, wavefront tilt in two axes for *each* interferometer arm, and internal metrology OPD.

The matrix B_f is defined to include the disturbance and the control actuation input. The IRU output are selected from the output of Eq. 11, by premultiplying by an appropriate matrix, C_{gyro}. The optical output are obtained by premultiplying d by the optical sensitivity matrix, C_{opt}. In this case the C matrix of the measurement equation of Eq. 11 becomes:

$$C = \begin{bmatrix} C_{opt} & 0 \\ C_{gyro} & \end{bmatrix} C_d \tag{14}$$

Note that the D matrix of Eq. 11 is still zero but now has different dimension.

Open-Loop Disturbance Analysis

The open-loop disturbance analysis is performed for three cases: 1) hardmounted RWA with no structural quieting, 2) isolated RWA with no structural quieting, and 3) hardmounted RWA with structural quieting. The results are shown in the subsequent figures, one of DWT and OPD in each case for a total of six. First, the analysis methodology and output are described. Next, the disturbance requirements are developed. Last, the isolation and structural quieting models are described and the results are given.

Disturbance Analysis Method

The disturbance analysis consists of exciting the integrated model with reaction wheel disturbance spectra in order to obtain stellar OPD and DWT. The reaction wheel disturbance spectra are generated from the narrowband model of the Hubble Space Telescope (HST) wheels described in [3]. This model is based on testing of the HST flight units.

Since the reaction wheel disturbances are a function of the reaction wheel speed, and since the reaction wheel speed will vary as described in [9], the disturbance analysis is parameterized according to wheel speed. That is, for each reaction wheel speed the root-mean-squared OPD and DWT variations for a single interferometer are found. This rms OPD or DWT is plotted as a function of wheel speed, (*e.g.*, Figure 6). Furthermore, in order to characterize the rms OPD and DWT over all wheel speeds with a single number, the root-mean-square of the parameterized optical metric over all wheel speeds is calculated (*i.e.*, the $\mathcal{L}_2$ norm). This metric may be confusing, and is discussed in more detail in [3]. The $\mathcal{L}_2$ norm is given in the y-axis label of the following figures.

Instead of performing the analysis with three or four wheels, making the wheel speed parameterization multi-dimensional, the analysis assumes a single wheel mounted with its axis in the z-direction (refer to Figure 4). The reaction wheel's orientation has little bearing on the resultant OPD and DWT. Variation of roughly a factor of two between wheel orientations along different coordinate axes has been observed with the SONATA integrated model, with the z-axis orientation being the worst case.

The DWT output of the model are DWT about the two axes in the plane of the detector, σ_x and σ_y. The quantity that affects the fringe visibility, however, is the the magnitude of the vector sum of the DWT about the two detector axes, known as the total DWT, σ_{DWT}:

$$\sigma_{DWT} = \sqrt{\sigma_x^2 + \sigma_y^2} \tag{15}$$

As a matter of preference, the OPD and DWT variation are given in terms of wavelengths of starlight. The reference wavelength, λ_o, is the center wavelength of the stellar interferometer, 550 nm. The conversion from OPD in meters, σ_{OPD}, and DWT in radians, σ_{DWT}, is according to:

$$\begin{aligned} \lambda_{OPD} &= \frac{\sigma_{OPD}}{\lambda_o} \\ \lambda_{DWT} &= \sigma_{DWT}\frac{d}{\lambda_o} \end{aligned} \tag{16}$$

where λ_{OPD} and λ_{DWT} are OPD and DWT in waves, and d is the beam width at the detector.

Pathlength and Wavefront Tilt Requirements

The OPD and DWT requirements derive from a stellar fringe visibility requirement of 90% [10]. Dividing this evenly between DWT and OPD the requirement for the contribution of each is 95% (*i.e.*, $0.9^{\frac{1}{2}}$). Since the disturbances resulting from different wheel orientations are roughly equivalent, the requirement is evenly divided among four RWAs, yielding a requirement for a single RWA of 98.7% for each of OPD and DWT.

Using Eq.17 for visibility, V, the requirements are converted into OPD and DWT variation in waves [10]. The OPD and DWT requirements for a single RWA in waves are $\lambda/39$ and $\lambda/10$, respectively. These correspond to 14 nm of OPD and 1.1 μrad of DWT. These requirements are represented in the subsequent disturbance analysis figures as a dashed line.

$$\begin{aligned} V &= e^{-\frac{1}{2}(2\pi\lambda_{OPD})^2} \quad \text{for OPD} \\ V &= e^{-1.23\lambda_{DWT}^2} \quad \text{for DWT} \end{aligned} \tag{17}$$

Disturbance Analysis Results

The OPD and DWT variation for the hardmounted RWA with no structural quieting are shown in Figures 6 and 7. Both OPD and DWT variation are well above the requirement for a large range of wheel speeds, particularly for higher wheel speeds. At worst, the OPD variation is two orders of magnitude larger than the requirement, and DWT variation is a factor of 20 larger.

The results for an isolated RWA without structural quieting are shown in Figures 8 and 9. In this case, the isolation was modeled by low-pass filtering the disturbance input in all six degrees of freedom. This filtering is consistent with a hexapod isolator, but it assumes that there are no dynamic interactions between the isolator and the rest of the structure. This is not actually the case, because the non-proportional damping in the struts will cause coupling between the hexapod modes and the modes of the structure. The effects of this coupling, however, may or may not be detrimental to the overall disturbance analysis as compared to the uncoupled model. This assumption simplified the modal truncation. The isolation model has a resonance of 4 Hz that is damped at 3% of critical [11]. The requirements are met for DWT and are met at all but the low wheel speeds for OPD variation. The low frequency peaks of the OPD variation correspond to excitation of the lightly damped isolator resonance.

The results for a hardmounted RWA with structural quieting are shown in Figures 10 and 11. The structural quieting was modeled by increasing the modal damping from 0.1% to 5% for all modes. This damping level is consistent with modal damping of the CSI Phase B testbed with optimally placed dampers for lower frequency modes (< 100 Hz) [1]. It is optimistic, however, for the higher frequency modes, because the damping struts impart damping primarily in the axial direction. They will provide very little damping of modes involving strut bending, regardless of placement. These modes are generally at higher frequency. This would tend to make the results worse, particularly for higher wheel speeds. The requirement is met for DWT, but is not met for OPD, although there is significant improvement.

The results for the three cases are summarized in Table 1.

Case	**OPD Variation**				**DWT Variation**			
	$\mathcal{L}_2$ norm		Max		$\mathcal{L}_2$ norm		Max	
	λ_o	nm	λ_o	nm	λ_o	nrad	λ_o	nrad
1	0.332	183	3	1,650	0.243	2,600	1.6	17,600
2	$8.42\text{x}10^{-3}$	4.63	0.07	39	$2.07\text{x}10^{-4}$	2.27	$1.7\text{x}10^{-3}$	21
3	$4.13\text{x}10^{-2}$	22.7	0.09	50	$1.74\text{x}10^{-2}$	191	$3.9\text{x}10^{-2}$	429
Reqmnt	—	—	$2.56\text{x}10^{-2}$	14	—	—	0.1	1,100

Table 1: Results of the Open-Loop Disturbance Analysis.

Conclusion and Future Work

An integrated structures-optics model has been described that enables end-to-end open-loop disturbance modeling. Furthermore, the model includes actuator input and sensor

output for the internal and stellar pathlength control, wavefront tilt control, and attitude control, allowing for closed-loop modeling.

This model has been used to perform an open-loop disturbance analysis, variously incorporating RWA isolation and structural quieting. OPD and DWT variation are used as optical performance metrics, and requirements are generated for both. The modeled disturbances are RWA vibrations. The disturbance analysis is parameterized by wheel speed, given that it may vary between observations.

Without any disturbance attenuation layers, the performance is up to two orders of magnitude worse than the requirement, with the problem in the moderate to high wheel speeds. When the RWA is isolated, the requirements are met for moderate and high wheel speeds, but are slightly exceeded for low wheel speeds. In this case the problem is the lightly damped resonance of the isolator itself. When structural quieting alone is used, the requirements are met for low and moderate wheel speeds, but are not met for high wheel speeds. Furthermore, the structural damping assumed for the higher frequency modes is optimistic.

Presently, closed-loop disturbance analyses of the wavefront tilt control system and the pathlength control systems are being performed. These analyses also incorporate closed-loop attitude control modeling. Further work ought to include: 1) a more detailed structural quieting analysis, using discrete damping elements and a damper placement and tuning design [12] and 2) an in-depth isolation design, incorporating non-proportional damping struts and investigating active isolation options [2].

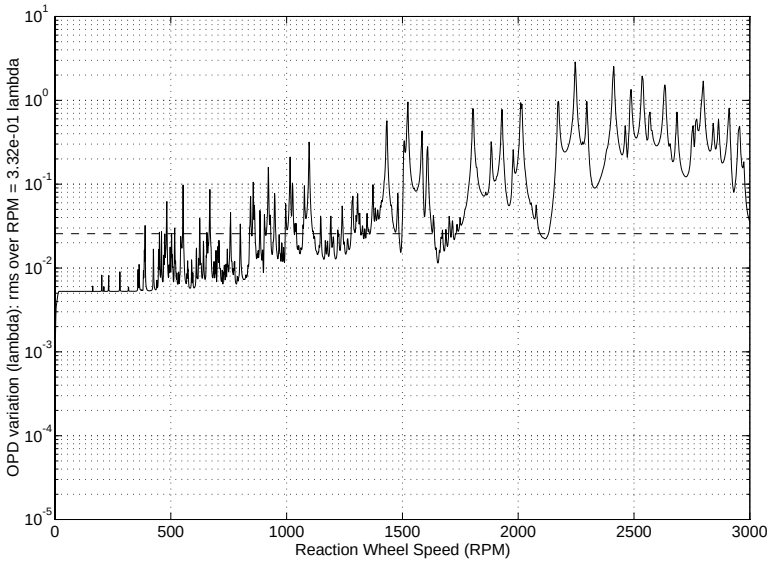

Figure 6: Case 1 - SONATA RWA Induced OPD Variation for Hardmounted RWA with no Structural Quieting

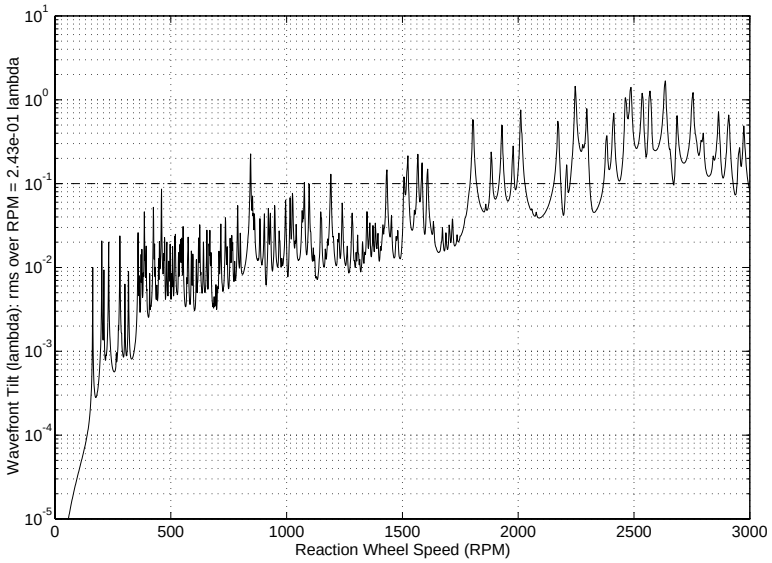

Figure 7: Case 1 - SONATA RWA Induced DWT Variation for Hardmounted RWA with no Structural Quieting

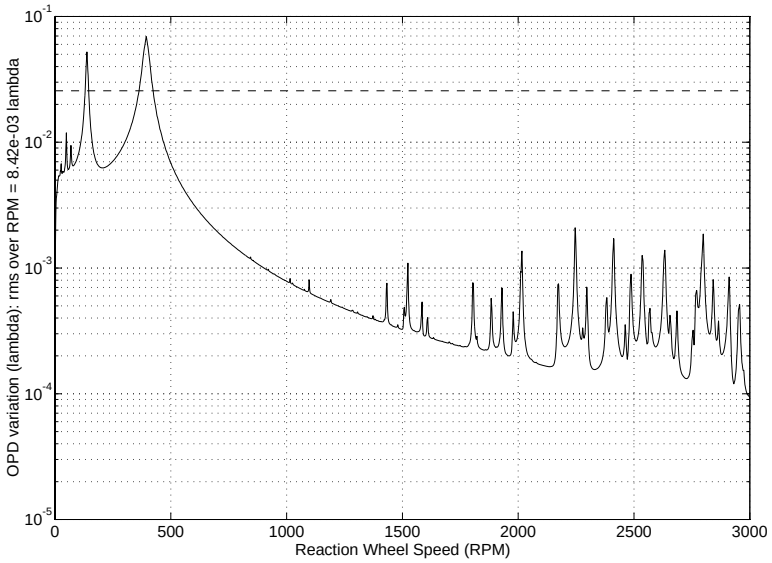

Figure 8: Case 2 - SONATA RWA Induced OPD Variation for Isolated RWA with no Structural Quieting

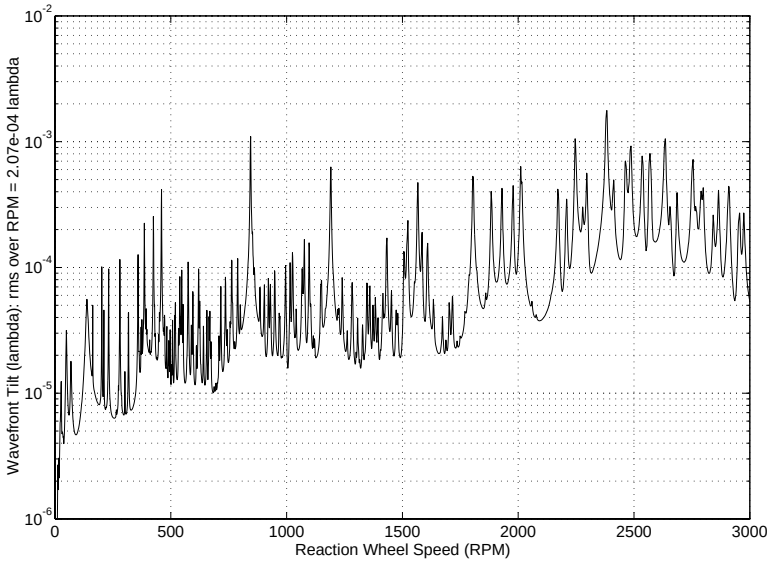

Figure 9: Case 2 - SONATA RWA Induced DWT Variation for Isolated RWA with no Structural Quieting

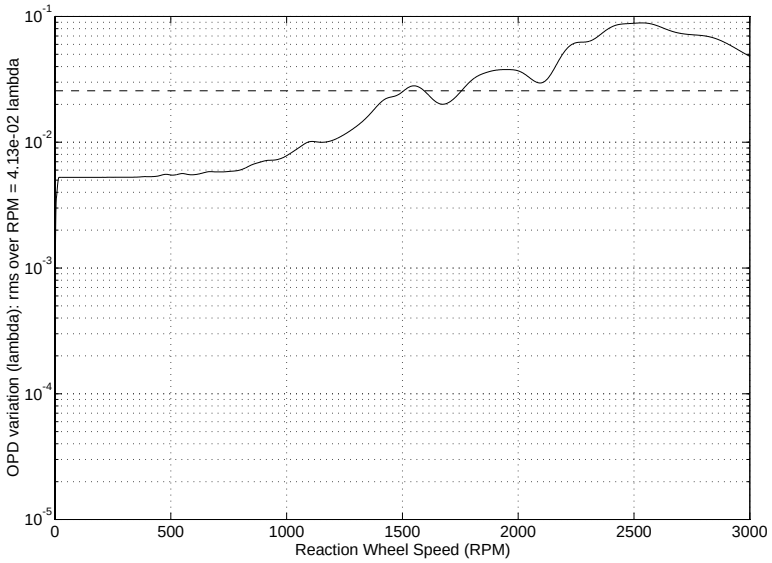

Figure 10: Case 3 - SONATA RWA Induced OPD Variation for Hardmounted RWA with Structural Quieting

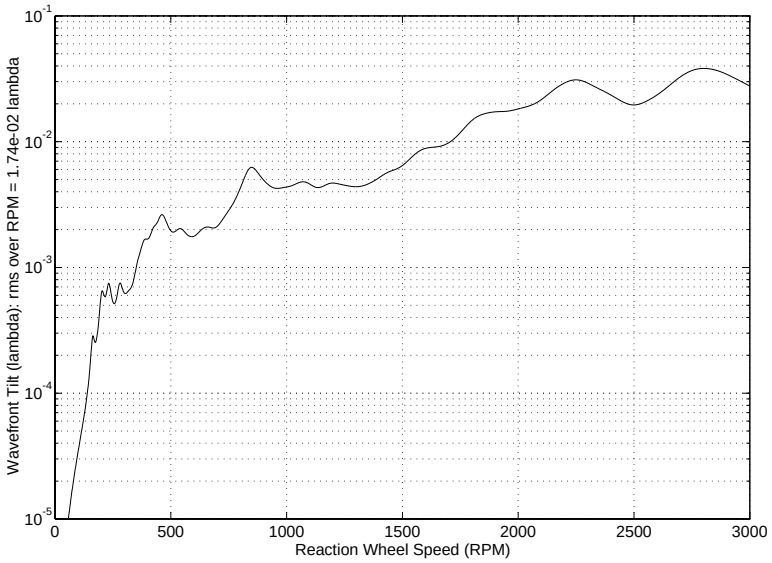

Figure 11: Case 3 - SONATA RWA Induced DWT Variation for Hardmounted RWA with Structural Quieting

References

1. J.Spanos, *et.al.*, "Control Structure Interaction in Long Baseline Interferometers," 12^{th} IFAC Symposium on Automatic Control in Aerospace, Ottobrun, Germany, September, 1992.

2. J.F.O'Brien, *et.al.*, "Six-Axis Vibration Isolation Technology Applied to Spaceborne Interferometers," 1995 SPIE International Symposium on Aerospace/Defense Sensing & Control and Dual-Use Photonics, Spaceborne Interferometry II Conference, Orlando, FL, April 1995.

3. J.W.Melody, "Discrete-Frequency and Broadband Reaction Wheel Disturbance Models," JPL IOM 3411-95-200csi, June 1,1995.

4. H.C.Briggs, "Integrated Modeling of Optical Systems User Guide, Release 1.0," June 1, 1992.

5. D.Redding, "Controlled Optics Modelling Package User Manual, Release 1.0," JPL D-9816, June 1, 1992.

6. C.Z.Gregory, Jr., "Reduction of Large Flexible Spacecraft Models using Internal Balancing Theory," *Journal of Guidance and Control*, Vol. 7, November- December 1984, pp. 725–732.

7. C.C.Chu, M.H.Milman, "Eigenvalue Error Analysis of Viscously Damped Structures Using a Ritz Reduction Method," *AIAA Journal*, Vol. 30, Number 12, December 1992, pp. 2935–2944.

8. E.Balmes, *Experimental/Analytical Predictive Models of Damped Structural Dynamics*, MIT Ph.D. Thesis, SERC #7-93, May 1993.

9. J.W.Melody, "SONATA Reaction Wheel Assembly (RWA) Angular Momentum Budget" JPL IOM 3411-94-1994, July 29, 1994.

10. M.Colavita, "Visibility and Phasing," JPL IOM, August 10, 1994.

11. D.Cunningham, P.Davis, F.Schmitt, "A Multiaxis Isolation System for the French Earth Observation Satellite's Magnetic Bearing Reaction Wheel," Proceedings of the ADPA/ AIAA/ASME/SPIE Conference on Active Materials and Adaptive Structures, Alexandria, VA, November 1991.

12. M.H.Milman, C.C.Chu, "Optimization Methods for Passive Damper Placement and Tuning," 1992 AIAA Guidance, Navigation, and Control Conference, Hilton Head, SC, August, 1992.